Pak. J. Chem. 16(3): 99-107, 2026 Research article
ISSN(Print):2220-2625
ISSN(Online):2222-307X DOI:10.15228/2026.v16.i3.p11

Low-Temperature Hydrothermal Synthesis of High-Performance Al–ZnO on Flexible, Durable, and Aligned hBN/Cu substrates

Humera Shaikh[1*], Ramsha Saleem[1], Muhammad Saajan Bharhaam[2], Abdul Majid Soomro[1], Waseem Ahmed Bhutto[1], Zahid Hussain Arain[1], Muhammad Waseem Mirbhar[1], Muhammad Ayaz Khoso[1]
[1] Institute of Physics, University of Sindh, Jamshoro 76080, Pakistan
[2] Mehran University Institute of Science & Technology Development, Jamshoro 76062, Pakistan
Corresponding Author email: humera-9@hotmail.com

Abstract
In this work, a low-temperature hydrothermal technique was successfully employed to synthesize pure Al-doped zinc oxide (ZnO) nanostructures on flexible hBN/Cu substrates.The structural and optical effects of Aluminum (Al) dopant concentrations ranging from 2 at% to 10 at% were investigated. SEM imaging revealed vertically oriented hexagonal nanowires (NWs) that grew larger and more densely as the doping level increased. A hexagonal wurtzite structure with a preferred (002) orientation at 34.462° was confirmed by XRD analysis. The optical bandgap showed a systematic redshift from 3.20 eV to 3.17 eV, and the grain size, determined by the Debye-Scherrer equation, decreased from 42.1 nm to 18.9 nm as the Al concentration increased. Al-doped ZnO nanostructures possess a tunable bandgap (3.20 eV to 3.17 eV) and prominent Near-Band Edge (NBE) UV emission, with increased doping levels reducing green emission, suggesting enhanced stoichiometry through vacancy passivation. The hBN buffer layer successfully prevents copper diffusion, as demonstrated by EDX, and the 10% Al-doped sample provides flexible UV sensors with a good balance between electrical conductivity and optical clarity. These results demonstrate that the Al-doped ZnO/hBN/Cu combination works as a robust, versatile electrode platform, bridging the gap between high-performance ceramics and wearable electronic devices.

Keywords: Al-ZnO Nanowires, hBN/Cu substrate, flexible electrodes, hydrothermal process, energy harvesting

1. Introduction

Nowadays, the most vital elements in optoelectronic devices are ZnO [1]. It has a wide direct bandgap and a high exciton binding energy of 3.37 eV and 60 meV, respectively [2]. Due to these properties, it is suitable for many applications, including photocatalysis [3], flexible energy harvesting [4], and UV sensors [5]. Usually, these nanostructures are designed on rigid substrates such as silicon or glass [6], but as wearable technology has advanced rapidly, interest has shifted to flexible metallic platforms [7]. The use of polymers coated with indium tin oxide (ITO) is a significant obstacle to the advancement of flexible electronics [8]. When bent, these traditional substrates experience microcracking and significant conductivity loss due to a severe mismatch in thermal expansion coefficients between the flexible polymer base and the rigid inorganic oxide layer. Additionally, ITO is very brittle and exhibits poor thermal stability during high-temperature processing, making it vulnerable to catastrophic mechanical failure under low-repetitive strain cycles [9]. Growing ZnO directly on Co using hydrothermal techniques usually results in substrate oxidation or poor crystal alignment, even though copper (Cu) foil offers higher flexibility and conductivity [10]. There is a significant research gap in the stable, high-quality synthesis of Al-doped ZnO (AZO) on flexible metallic foils, as most current investigations focus on either rigid substrates or brittle polymers [11]. In this work, we use hexagonal boron nitride (hBN) as an essential intermediate buffer layer to overcome these difficulties [12]. Two main factors led to the selection of hBN. It encourages epitaxial-like growth and vertical alignment of nanowires because its hexagonal symmetry closely resembles that of ZnO [13]. During the hydrothermal process, it serves as a strong, atomically thin shield to prevent oxidation of the underlying Cu [14]. We expect that the addition of a hBN layer will greatly enhance the mechanical and thermal resilience of the AZO nanowire arrays, while preventing substrate degradation [15-18].

Additionally, higher Al dopant concentrations are expected to enable precise control over crystalline grain size and optical bandgap, thereby enhancing the material's suitability for specific electrode applications. The effective incorporation of Al doping into an hBN/Cu heterostructure through an economical, low-temperature hydrothermal method distinguishes this study from earlier research. This work also provides a foundation for the development of flexible piezoelectric energy harvesters and self-powered wearable sensors that can withstand the mechanical demands of everyday human motion.

2.0. Materials and Methods

2.1. Chemicals and Reagents

Al-doped ZnO nanowire arrays were fabricated using a scalable, economical bottom-up hydrothermal method. Every chemical precursor, including hexamethylenetetramine (HMT) and zinc nitrate hexahydrate, was of analytical grade (Sigma-Aldrich, 99.9% purity).

2.2. Substrate Engineering and Preparation

The growth platform consists of flexible Copper (Cu) foil pre-coated with an atomically thin layer of hexagonal Boron Nitride (hBN) [19]. The hBN serves a dual purpose: acting as a template for epitaxial-like growth and as a chemical diffusion barrier [20]. The hBN/Cu substrates were treated according to a careful multi-stage cleaning procedure to

provide a perfect nucleation surface [21]. After 15 minutes of ultrasonic cleaning in high-purity Deionized (DI) water to remove surface dust, the foils were rinsed for 10 minutes in absolute ethanol to remove any organic residue. To avoid pre-synthesis oxidation, the substrates were finally dried under a constant stream of ultra-high-purity nitrogen (N_2) [22].

2.2.2. Doping Protocol

Calculated stoichiometric amounts of aluminum nitrate nonahydrate were added to the growth solution in order to examine the impact of Aluminum (Al) concentration. To achieve doping levels of 0, 2, 4, 8, and 10 %, at five different concentrations were made. This systematic variation enables the precise study of changes in structural and optical properties.

2.2.3. The "Float-Face-Down" Growth Technique

The hBN/Cu substrates were arranged "float-face-down" inside the reaction vessel, with the hBN-coated side facing downward; they were placed on the liquid's surface in this orientation. This strategy is crucial for two reasons: it uses gravity to prevent bulk precipitates from building up on the growth surface and disrupting nanowire alignment [23]. It states that the diffusion of ions to the interface controls growth, promoting stable, high-density vertical alignment across the entire substrate surface [24]. For three hours, the beakers were sealed and maintained at 90 °C in a lab oven. Following the growth period, the samples were removed, thoroughly rinsed with DI water to remove residual ions, and air-dried at room temperature (Fig. 1).

(2.9 gm) Zinc nitrate hexahydrate added with (1.4 gm) HMT in 200 ml D.I. water.

Stirring the solution for 1 hr.

Kept in oven for 3 hrs at 90 °C for the growth of Al-doped ZnO nanowires

Figure 1: The schematic diagram of the experimental procedure.

A precursor solution was prepared for the baseline undoped sample by dissolving 2.9 gm of zinc nitrate hexahydrate and 1.4 gm of HMT in 200 mL of DI water. To achieve a perfectly homogeneous, transparent solution, the mixture was continuously stirred magnetically at 500 rpm for 60 minutes at room temperature.

2.3. Structural Studies

To meet the rigorous requirements of modern materials science, Al-ZnO on a hBN/Cu substrate was characterized using the following parameters. Scanning Electron Microscopy was employed to analyze the nanowire dimensions and nucleation density from high-resolution images at an accelerating voltage of 10kV and a magnification of 10,000x. X-Ray Diffraction was performed using a PANalytical X'Pert PRO diffractometer equipped with Cu-Kα radiation (1.5406 Å), operating at 40 kV and 40 mA, collected over 10° to 80° with a step size of 0.02°. Optical analysis was performed at room temperature using photoluminescence spectroscopy with a PerkinElmer LS45 Fluorescence Spectrometer. The samples were tested at room temperature using an excitation wavelength in the UV range. The emission spectra were recorded from 300 nm to 700 nm with a scanning speed of 800 nm/min. Elemental composition was analyzed by energy-dispersive X-ray spectroscopy to validate quantitative stoichiometry [25].

3.0. Results and Discussion

3.1. Surface Morphology and Growth Mechanism

Scanning Electron Microscopy was used to observe the surface morphology, alignment, and structural development of the pure and Al-doped ZnO (AZO) nanostructures (Fig.2a-e). The micrographs show that on the flexible hBN/Cu substrate, the ZnO nanowires (NWs) are primarily oriented vertically.

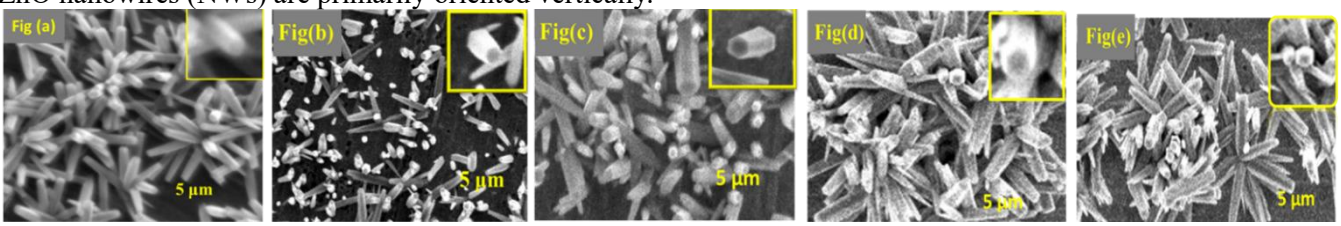

Figure 2: SEM images of pure and Al-doped ZnO NWs with the different concentrations, (a) Pure ZnO, (b) 2%, (c) 4%, (d) 8%, (e) 10%.

The hexagonal symmetry of the hBN buffer layer is the main cause of the vertical alignment seen in all samples [26]. As a structural template that reduces interfacial energy during the first nucleation stage, the lattice constant of hBN offers a near-epitaxial match for the (0001) plane of ZnO [27]. The hBN layer serves as an atomically thin oxidation barrier, maintaining the conductivity of the Cu foil while promoting c-axis growth, in contrast to growth on bare Cu, which often leads to random orientation and substrate oxidation [28]. Table (1) summarizes the morphological parameters of AZO nanowires (NWs), showing an increase in average Diameter (~80 nm to ~150 nm) and length (~1.2 µm to ~2.5 µm) as aluminum doping increases from 0% to 10 %. This data demonstrates a shift in nucleation density from a moderate to a

dense "bulk quantity" of vertically aligned nanowires, highlighting a relationship between Al concentration and growth kinetics [29]. The NWs exhibit a unique facet-hexagonal wurtzite cross-section at lower concentrations. The SEM (Fig 2, "d" and "e") shows a shift to a "bulk quantity" forest of nanowires at higher doping levels. Al ions are thought to function as surfactants or capping agents during the hydrothermal process [30].

Table 1: shows the morphological dimensions of AZO NWs

Sample (at%)	Average Diameter (nm)	Average length (µm)	Nucleation Density
Pure ZnO	~80	~1.2	Moderate
2% Al-ZnO	~95	~1.5	Moderate
4% Al-ZnO	~110	~1.8	High
8% Al-ZnO	~135	~2.1	Bulk/Very High
10% Al-ZnO	~150	~2.5	Bulk Quantity

Al ions prevent lateral expansion and reroute the chemical potential toward longitudinal growth along the (0001) direction by preferentially adsorbing on the non-polar side walls of the ZnO crystals [31]. This leads to increases in length and aspect ratio observed at 10 % doping. For the suggested application in self-powered wearable sensors, the change from sparse NWs to a dense, high-surface-area forest is important [32]. At 10% doping, the higher nucleation density results in a much larger electrochemical surface area, thereby improving charge-collection efficiency [33]. The vertical orientation ensures that the NWs can "fan out" rather than crack when the Cu foil is twisted, a typical failure mode in brittle ITO thin films [11,34]. By offering a linear, one-dimensional path for electron transport from the NW's tip to the Cu electrode, the alignment reduces internal series resistance and speeds up UV sensor response times [35]. The basis for a wearable sensor with great sensitivity is the shift to a "bulk quantity" of vertically aligned nanowires at 10% Al-doping. We optimize the area accessible for mechanical contact or photon absorption by increasing the surface-to-volume ratio [36]. The vertical orientation ensures a "shortest-path" for electron transport to the Cu foil, thereby shortening reaction times and enabling real-time, signal-lag-free tracking of human movements [7].

3.2. Crystallographic Analysis (XRD)

X-ray diffraction (XRD) was used to examine the crystalline structure and phase purity of the produced pure and Al-doped ZnO nanowires. All samples have a hexagonal wurtzite structure, which is compatible with the standard JCPDS card no. 36-1451, according to the patterns shown in Figure 3(a) [37]. The figure shows the XRD patterns of ZnO and Al-doped ZnO nanowires with different concentrations (2%, 4%, 8%, and 10%) grown on a flexible hBN/Cu substrate by the hydrothermal method. The typical shift of the main (002) peak toward higher diffraction angles as the Al concentration increases is a significant observation in the XRD data [38]. All the diffraction peaks correspond well to pure; no significant shift is observed. The (002) peaks of all patterns show higher intensity than the other peaks at angles of 43°, 52° & 75°. Very sharp, intense peaks indicate that the crystalline quality of pure and Al-doped ZnO nanowires is good, with uniform c-axis orientation [39], which is influenced by the orientation of the hBN buffer layer. The peak shifts from 34.462° (pure ZnO) to 34.52° (10% Al-ZnO), as observed experimentally. This shift indicates substitutional doping [40].

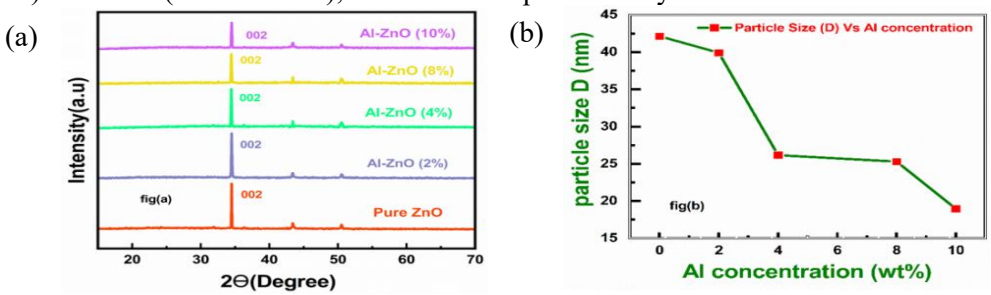

Figure 3: (a) shows the XRD pattern of Pure and Al- ZnO arrays with different Al doping concentrations of 2%, 4%, 8%, and 10%, respectively. (b) shows the relationship between Al concentration vs particle size.

3.2.1. Crystallite Size and FWHM Trends

The crystallization quality was further quantified using the Debye-Scherrer equation.

$$d = \frac{0.89\lambda}{\beta \cos\theta}$$

Here, λ, β, and θ represent the wavelength of the X-ray radiation (1.54056 Å), the full width at half maximum (FWHM) of the peak, and the diffraction angle, respectively [41].

The decrease in particle size, which ranges from 42.13 nm to 18.95 nm, is clearly correlated with the concentration of Al, as reported in Table (2). A reduction in the long-range crystalline order is suggested with an increase in FWHM (from 0.18 to 0.40) [36]. The formation of smaller, larger crystalline structures results from the addition of Al dopants, which create point defects and small stress fields that prevent the growth of large crystals [42]. This decrease in particle size is highly beneficial for the hBN/Cu flexible substrate from a mechanical perspective [43]. Grain boundaries, which act as "hinges" that allow the nanostructured material to resist mechanical strain while bending, are common in smaller grains [44]. This explains why the 10% Al-doped sample is expected to show the highest resilience to cracking in wearable

applications, as the "finer" grain structure can distribute stress more effectively than the larger, more brittle grains of pure ZnO.

Table 2: Calculated Structural Parameters of Pure and Al-doped ZnO NWs

Sample	2θ (Degree)	d-spacing (nm)	FWHM (Degree)	Grain Size (nm)
Pure ZnO	34.462	0.2599	0.18	42.13
2% Al-ZnO	34.472	0.2598	0.19	39.91
4%Al-ZnO	34.482	0.2597	0.29	26.15
8% Al-ZnO	34.499	0.2596	0.30	25.28
10% Al-ZnO	34.520	0.2595	0.40	18.95

The reduction in grain size (from 42 nm to 18 nm), (Fig. 3b) is the key to mechanical durability. Large grains are prone to "cleavage" and cracking under stress. By engineering a "fine-grain" structure via Al doping, we create a more flexible nanostructured film [45]. This ensures that when a wearable patch is applied to a moving joint (such as an elbow or knee), the electrode remains electrically continuous and does not experience "fatigue cracking" from repeated bending cycles.

3.4. Photoluminescence properties of pure and Al-doped ZnO NW's

The optical properties and electronic transitions of the pure and Al-doped ZnO nanowires were investigated using PL spectroscopy at room temperature. As illustrated in the spectra (Figure 4a) two distinct emission regions are observed: a sharp, dominant Near-Band Edge (NBE) emission in the UV region (~370–390 nm) and a suppressed Deep Level Emission (DLE) in the visible green region (~500–560 nm) [46]. The NBE emission originates from the recombination of free excitons. The steady redshift of the NBE peak position as the aluminum content increases from 0 to 10 at% is a critical finding of this study. From the calculations, the optical bandgap narrowed from 3.20 eV to 3.17 eV [47]. Two different systems control this phenomenon: ions act as shallow donors at high doping levels, providing an abundance of free electrons that occupy the lower conduction-band states. Normally, combining these elements results in a blue shift [48]. However, because these samples are so densely packed with excess electrons, they begin to interact with each other and with the material's impurities [49]. These interactions actually reduce the energy gap between the material's layers, resulting in a red shift instead [50]. The point is that the 10% aluminum synthesis reached a high-doping level, indicating that it has become an excellent electrical conductor.

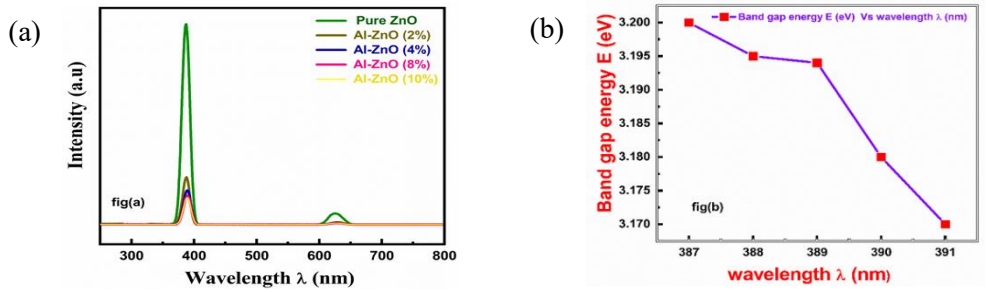

Figure 4: (a) Photoluminescence (PL) spectra of the hydrothermally grown pristine and Al-ZnO nanowires on flexible hBN/Cu substrate with the different concentrations of aluminum, like (2%, 4%, 8%, 10%). (b) Relation between wavelength and bandgap.

3.3.1. Defect States and Stoichiometry (DLE)

Zinc interstitials and oxygen vacancies are commonly linked to the "Green Emission" (DLE). Our results demonstrate that the intensity of the green emission decreases with increasing Al content [51]. This implies that ions either passivate grain boundaries or occupy the vacant oxygen sites. By improving the crystal's stoichiometry, this "defect engineering" creates a more stable electrical structure. For self-powered UV sensors, this optical tuning is highly desirable [52]. The sensor is highly sensitive, absorbing particular UV-A radiation while remaining transparent to visible light due to a narrower, more precise bandgap at 3.17 eV [52]. Furthermore, electron trapping was minimized by suppressing green emission via reduced oxygen vacancies. In a wearable sensor, this means the device will have a faster recovery time and a higher signal-to-noise ratio, ensuring accurate detection of UV exposure without interference from indoor ambient lighting [54].

3.3.2. Bandgap investigation using photoluminescence

The optical bandgap (Eg) was calculated from the NBE emission peak position using the following relation in order to address the optical behavior.

$$E_g = hc/\lambda,$$

where "λ" is the emission wavelength, "c" is the speed of light, and "h" is Planck's constant [55]. The bandgap for undoped ZnO was determined to be 3.20 eV. Figure 4(b) illustrates a systematic red shift in the NBE peak following the addition of Al to ZnO, with the bandgap falling to 3.20 eV, 3.19 eV, 3.18 eV, and 3.17 eV for samples Al-ZnO 2%, 4%, 8%, and 10%,bandgap.

3.4. Compositional Analysis (EDX)

Elemental composition was analyzed by energy-dispersive X-ray spectroscopy (EDX) to validate quantitative stoichiometry and verify successful dopant integration into the host lattice [56]. The quantitative results verify the

proportional incorporation of Aluminum (Al) into the Zinc Oxide (ZnO) matrix. The EDX spectra summarized in Table 3 show distinct peaks for Zinc (Zn), Oxygen (O), and Aluminum (Al). As the Al concentration increases, it does so consistently with the precursor concentration (2% to 10%). The atomic percentage of Al was found to be in close agreement with the intended doping levels, confirming the high efficiency of the hydrothermal synthesis.

Table 3: Quantitative Elemental Composition (Atomic %)

Sample	Zn (%)	O (%)	Al (%)	B (%)	N (%)
Pure ZnO	51.2	48.8	-	~2.1*	~1.9*
2% Al-ZnO	49.8	48.2	2.0	~2.0*	~2.0*
10% Al-ZnO	42.1	47.9	10.0	~1.8*	~1.8*

*Signal from the underlying hBN buffer layer

3.4.1. Integrity of the hBN/Cu Interface

Significant findings include the absence of visible Cu peaks in the upper nanostructure layers and the distinct signals from boron (B) and nitrogen (N) in the EDX data. This suggests that the hexagonal Boron Nitride (hBN) layer was unaffected by the 3-hour hydrothermal treatment at 90 °C [57]. The EDX results reveal that hBN has a completely impenetrable barrier. In conventional ZnO growth on Cu, Cu atoms often migrate into the ZnO lattice, creating metallic impurities that "short-circuit" the structure. In this case, hBN maintains the electrical purity of the nanowires by acting as a chemical barrier that prevents copper from migrating [58]. This chemical stability is the "core" of a durable and enduring wearable sensor. In the real world, wearable gadgets come into contact with human sweat, which contains ions that can corrode copper. Our EDX results show that the hBN layer is a robust barrier, protecting our device from internal corrosion. This implies that the electrode will maintain steady electrical conductivity and a consistent signal for long-term health monitoring, even under challenging environmental conditions or during vigorous physical activity.

Future Perspectives of Current Research

Future uses of Al-doped Zinc Oxide (ZnO) nanostructures on hBN/Cu substrates will mostly focus on flexible, high-performance electronics. The main future applications are as follows:

Wearable Electronic Devices

These materials are ideal for "smart" apparel or skin-integrated electronics that require flexibility and durability, as they are synthesized on flexible substrates.

Flexible UV Sensors

According to the text, it has a "good balance between electrical conductivity and optical clarity," which makes it is a top contender for ultraviolet light detectors with high sensitivity and flexibility.

Robust Electrode Platforms

It can bridge the gap between conventional rigid ceramics and next-generation flexible technology by acting as a flexible electrode for a variety of optoelectronic devices.

Advanced Optoelectronics

The prominent "Near-Band Edge (NBE) UV emission" and "tunable bandgap" enable the creation of custom LEDs and laser diodes with particular energy or color outputs.

4.0 Conclusion

In conclusion, the integration of Al-doped ZnO nanowires with a flexible hBN/Cu heterostructure effectively addressed the severe limitations of brittle ITO-coated polymers, particularly their low thermal threshold and susceptibility to bending-induced microcracking, as well as metal-substrate oxidation [8, 11]. The hBN buffer layer played a crucial dual role, promoting an epitaxial-like vertical alignment of the nanowires along the c-axis while preventing copper oxidation and degradation. Al^{3+} ions were effectively incorporated into the ZnO lattice, [59] resulting in a controlled reduction in grain size and improved stoichiometric stability, as confirmed by XRD and EDX analyses. These morphological modifications significantly enhanced the electrode's active surface area and charge-collection efficiency, particularly through the formation of a dense, highly aligned nanowire array at 10 at% Al doping. Furthermore, the optical bandgap could be precisely tuned by varying the Al concentration, enabling customization for UV sensing and optoelectronic applications. The reduced grain size and vertical orientation facilitated low-resistance carrier transport and improved flexibility under repeated bending, making the structure both mechanically durable and electrically conductive. The scalable and cost-effective hydrothermal approach also demonstrates strong potential for the fabrication of fully flexible piezoelectric energy harvesters and self-powered wearable sensors. Overall, the AZO/hBN/Cu platform represents a reliable and efficient candidate for next-generation durable wearable electronics and advanced optoelectronic devices.

Acknowledgment

The Authors would like to thank the Institute of Physics at the University of Sindh for providing the facilities and technical support necessary to complete this research.

Author's Contribution

Humera Shaikh (Conceptualization, investigation, methodology, formal analysis, data curation, validation, writing original draft, and editing), Ramsha Saleem (Investigation, validation, and editing), Muhammad Sajaan Bharhaam (editing and validation), Abdul Majid Soomro (Supervision, review, and validation), Waseem Ahmed Bhutto (Supervision,

review, and validation), Nek Muhammad Shaikh (Supervision, review, and validation), Muhammad Waseem Mirbhar(Visualization), Muhammad Ayaz Khoso (Visualization)

Conflict of Interest

The authors declare no conflict of interest

Funding Resource

NA.

References

1. Mohamed, M., Jaradat, E. K., Alshammari, A. S., & Sedky, A. (2025). Enhanced optical, dielectric and ferromagnetic properties in ZnO/M nanocomposites for advanced device applications. Scientific Reports, 15(1), 40353. https://doi.org/10.1038/s41598-025-26399-x
2. Saleem, R., Shaikh, H., Bharhaam, M. S., Soomro, A. M., Shaikh, N. M., Bhutto, W. A., Sanjrani, I. A., Arain, Z. H., Mirbhar, M. W., & Siyal, T. A. (2026). Mg-Induced Structural Transitions and Blue-Shift in the Optical Properties of ZnO. 16(3), 74–83. https://doi.org/10.15228/2026.v16.i3.p08
3. Kumari, S., Sharma, K., Korpal, S., Dalal, J., Kumar, A., Supreet, Kumar, S., & Duhan, S. (2024). A comprehensive study on photocatalysis: materials and applications. CrystEngComm, 26(35), 4886–4915. https://doi.org/10.1039/D4CE00630E
4. Kumar, B., & Kim, S.-W. (2012). Energy harvesting based on semiconducting piezoelectric ZnO nanostructures. Nano Energy, 1(3), 342–355. https://doi.org/https://doi.org/10.1016/j.nanoen.2012.02.001
5. Qin, L., Mawignon, F. J., Hussain, M., Ange, N. K., Lu, S., Hafezi, M., & Dong, G. (2021). Economic Friendly ZnO-Based UV Sensors Using Hydrothermal Growth: A Review. Materials (Basel, Switzerland), 14(15). https://doi.org/10.3390/ma14154083
6. Valerini, D., Caricato, A. P., Lomascolo, M., Romano, F., Taurino, A., Tunno, T., & Martino, M. (2008). Zinc oxide nanostructures grown by pulsed laser deposition. Applied Physics A, 93(3), 729–733. https://doi.org/10.1007/s00339-008-4703-z
7. Cheng, M. (2026). Research Progress of Wearable Flexible Sensors. 0, 224–238. https://doi.org/10.54254/2755-2721/2026.BJ32219
8. Ranka, A., Layek, M., Kochiyama, S., López Pernía, C., Chandler, A., Kocoj, C., Magliano, E., Carlo, A., Brunetti, F., Guo, P., Suresh, S., Paine, D., & Padture, N. (2025). Cracking in polymer substrates for flexible devices and its mitigation. https://doi.org/10.48550/arXiv.2504.18553
9. Shin, H.-C., Jang, Y., Kim, T.-H., Lee, J.-H., Oh, D.-H., Ahn, S. J., Lee, J. H., Moon, Y., Park, J.-H., Yoo, S. J., Park, C.-Y., Whang, D., Yang, C.-W., & Ahn, J. R. (2015). Epitaxial Growth of a Single-Crystal Hybridized Boron Nitride and Graphene Layer on a Wide-Band Gap Semiconductor. Journal of the American Chemical Society, 137(21), 6897–6905. https://doi.org/10.1021/jacs.5b03151
10. Huang, L., Wang, X., Yin, F., Zhang, Y., Gao, J., Liu, J., Zhou, G., & Bakenov, Z. (2016). ZnO Nanorods Grown Directly on Copper Foil Substrate as a Binder-Free Anode for High Performance Lithium-Ion Batteries. International Journal of Electrochemical Science, 11(10), 8439–8446. https://doi.org/https://doi.org/10.20964/2016.10.60
11. Jeong, J.-A., Shin, H.-S., Choi, K.-H., & Kim, H.-K. (2010). Flexible Al-doped ZnO films grown on PET substrates using linear facing target sputtering for flexible OLEDs. Journal of Physics D: Applied Physics, 43(46), 465403. https://doi.org/10.1088/0022-3727/43/46/465403
12. Park, A.-H., & Seo, T.-H. (2023). Hexagonal Boron Nitride as an Intermediate Layer for Gallium Nitride Epitaxial Growth in Near-Ultraviolet Light-Emitting Diodes. In Materials (Vol. 16, Number 22, p. 7216). https://doi.org/10.3390/ma16227216
13. Song, W., Liu, D., Wang, F., & Zhang, L. (2025). The Development of Hexagonal Boron Nitride Crystal Growth Technologies and Their Applications in Neutron Detection. In Nanomaterials (Vol. 15, Number 16, p. 1256). https://doi.org/10.3390/nano15161256
14. Indhu, A. R., Minakshi, M., Sivasubramanian, R., & Dharmalingam, G. (2025). A Focus on Thermal Durability and Oxidation Resistance and Morphology of Polymer Capped Copper Particles Through a Synthesis-Driven, Precursor-Influenced Approach. In Nanomaterials (Vol. 15, Number 24, p. 1852). https://doi.org/10.3390/nano15241852
15. Fukamachi, S., Solís-Fernández, P., Kawahara, K., Tanaka, D., Otake, T., Lin, Y.-C., Suenaga, K., & Ago, H. (2023). Large-area synthesis and transfer of multilayer hexagonal boron nitride for enhanced graphene device arrays. Nature Electronics, 6(2), 126–136. https://doi.org/10.1038/s41928-022-00911-x
16. Daira, R., Boudjema, B., Bououdina, M., Aida, M. S., & Constantinescu, C.-D. (2023). Influence of Al Doping on the Physical Properties of CuO Thin Films. In Applied Sciences (Vol. 13, Number 14, p. 8193). https://doi.org/10.3390/app13148193

17. Hassan, J., Naz, S., Haider, A., Raza, A., Ul-Hamid, A., Qumar, U., Haider, J., Goumri-Said, S., Kanoun, M. B., & Ikram, M. (2021). h-BN nanosheets doped with transition metals for environmental remediation; a DFT approach and molecular docking analysis. Materials Science and Engineering: B, 272, 115365. https://doi.org/https://doi.org/10.1016/j.mseb.2021.115365
18. Ali, A., Iqbal, S., & Chen, X. (2024). Recent advances in piezoelectric wearable energy harvesting based on human motion: Materials, design, and applications. Energy Strategy Reviews, 53, 101422. https://doi.org/https://doi.org/10.1016/j.esr.2024.101422
19. Han, G., Zhang, D., Kong, C., Zhou, B., Shi, Y., Feng, Y., Liu, C., & Wang, D.-Y. (2022). Flexible, thermostable and flame-resistant epoxy-based thermally conductive layered films with aligned ionic liquid-wrapped boron nitride nanosheets via cyclic layer-by-layer blade-casting. Chemical Engineering Journal, 437, 135482. https://doi.org/https://doi.org/10.1016/j.cej.2022.135482
20. Hu, J., Dong, M. Recent advances in two-dimensional nanomaterials for sustainable wearable electronic devices. J Nanobiotechnol 22, 63 (2024). https://doi.org/10.1186/s12951-023-02274-7
21. Chang, R.-J., Wang, X., Wang, S., Sheng, Y., Porter, B., Bhaskaran, H., & Warner, J. H. (2017). Growth of Large Single-Crystalline Monolayer Hexagonal Boron Nitride by Oxide-Assisted Chemical Vapor Deposition. Chemistry of Materials, 29(15), 6252–6260. https://doi.org/10.1021/acs.chemmater.7b01285
22. Li, Z., Wang, Z., Zhang, Q., Bai, X., Peng, L., Liu, C., & Yao, Z. (2025). Research progress on the epitaxial growth of hexagonal boron nitride on different substrates by the CVD method. Nanoscale Adv., 7(9), 2395–2417. https://doi.org/10.1039/D4NA00477A
23. Elezz, M. A., Aboeleneen, N. M., Abd-ElMonem, N. M., & Sorour, F. H. (2025). A comprehensive review: Functional nanomaterials for renewable energy: Innovations, applications, and sustainable strategies. Next Materials, 9, 101001. https://doi.org/https://doi.org/10.1016/j.nxmate.2025.101001
24. Yan, S., Lu, L., Meng, H., Huang, N., & Xiao, Z. (2010). Scalable alignment and transfer of nanowires based on oriented polymer nanofibers. Nanotechnology, 21(9), 95303. https://doi.org/10.1088/0957-4484/21/9/095303
25. Engineering, E. (2017). Growth and Characterisation of Au Colloid Catalysed Zinc Oxide Nanowires. August 2016.
26. Chen, J., Tao, R., Wang, G., Yin, Z., Zeng, L., Yu, X., Zhang, S., Wu, Y., Li, Z., & Zhang, X. (2023). The interface microstructure and band alignment of hexagonal boron nitride/diamond heterojunctions. J. Mater. Chem. C, 11(16), 5324–5330. https://doi.org/10.1039/D3TC00498H
27. Wang, M., Jang, S. K., Jang, W.-J., Kim, M., Park, S.-Y., Kim, S.-W., Kahng, S.-J., Choi, J.-Y., Ruoff, R. S., Song, Y. J., & Lee, S. (2013). A Platform for Large-Scale Graphene Electronics – CVD Growth of Single-Layer Graphene on CVD-Grown Hexagonal Boron Nitride. Advanced Materials, 25(19), 2746–2752. https://doi.org/https://doi.org/10.1002/adma.201204904
28. Kim, K. K., Hsu, A., Jia, X., Kim, S. M., Shi, Y., Hofmann, M., Nezich, D., Rodriguez-Nieva, J. F., Dresselhaus, M., Palacios, T., & Kong, J. (2012). Synthesis of Monolayer Hexagonal Boron Nitride on Cu Foil Using Chemical Vapor Deposition. Nano Letters, 12(1), 161–166. https://doi.org/10.1021/nl203249a
29. Barwich, S., Medeiros de Araújo, J., Rafferty, A., Gomes da Rocha, C., Ferreira, M. S., & Coleman, J. N. (2021). On the relationship between morphology and conductivity in nanosheet networks. Carbon, 171, 306–319. https://doi.org/https://doi.org/10.1016/j.carbon.2020.09.015
30. Li, X., Sun, M., Shan, C., Chen, Q., & Wei, X. (2018). Mechanical Properties of 2D Materials Studied by In Situ Microscopy Techniques. Advanced Materials Interfaces, 5(5), 1701246. https://doi.org/https://doi.org/10.1002/admi.201701246
31. Yang, D., Dai, P., Jiang, X., Alshehri, S. M., Ahamad, T., Bando, Y., & Wang, X. (2024). Methods for Preparation of Hexagonal Boron Nitride Nanomaterials. Chemistry of Materials, 36(20), 10008–10053. https://doi.org/10.1021/acs.chemmater.4c00582
32. Rayegani, A., Saberian, M., Delshad, Z., Liang, J., Sadiq, M., Nazar, A. M., Mohsan, S. A., & Khan, M. A. (2023). Recent Advances in Self-Powered Wearable Sensors Based on Piezoelectric and Triboelectric Nanogenerators. In Biosensors (Vol. 13, Number 1, p. 37). https://doi.org/10.3390/bios13010037
33. Kodan, N., Ahmad, M., & Mehta, B. R. (2020). Enhanced photoelectrochemical response and stability of hydrogenated ZnO nanorods decorated with Fe2O3 nanoparticles. Journal of Alloys and Compounds, 845, 155650. https://doi.org/https://doi.org/10.1016/j.jallcom.2020.155650
34. Rogdakis, K., Psaltakis, G., Fagas, G., Quinn, A., Martins, R., & Kymakis, E. (2024). Hybrid chips to enable a sustainable internet of things technology: opportunities and challenges. Discover Materials, 4(1), 4. https://doi.org/10.1007/s43939-024-00074-w
35. Han, S., Choi, I., Lee, C.-R., Jeong, K.-U., Lee, S.-K., & Kim, J. S. (2020). Fast Response Characteristics of Flexible Ultraviolet Photosensors with GaN Nanowires and Graphene. ACS Applied Materials & Interfaces, 12(1), 970–979. https://doi.org/10.1021/acsami.9b13109

36. Singh, N. J., Basumatary, I., Kolli, C. S. R., & Sahatiya, P. (2025). Current trends and emerging opportunities for 2D materials in flexible and wearable sensors. Chemical Communications, 61(60), 11158–11186. https://doi.org/https://doi.org/10.1039/d5cc02955d
37. Hossain, M. K., Al-Saadi, A. A., & Khan, F. (2025). Silver nanoparticles-embedded zinc oxide microbars as SERS-active substrates. Optics & Laser Technology, 189, 113062. https://doi.org/https://doi.org/10.1016/j.optlastec.2025.113062
38. Vishunumurthy, G., & Bhaskar, A. (2025). A Comprehensive Study on the Impact of Aluminum Doping on X-ray Diffraction Peak Profile Analysis, Structural, Morphological, and Optical Properties of ZnO Nanoparticles Synthesized by Sol–Gel Auto-Combustion. Journal of Electronic Materials, 54(3), 2146–2166. https://doi.org/10.1007/s11664-024-11636-2
39. Alonizan, N. H. (2022). Photoluminescence properties of Al-doped ZnO synthesized via facile sol-gel route. Journal of Alloys and Compounds, 912, 165084. https://doi.org/https://doi.org/10.1016/j.jallcom.2022.165084
40. Madhavi, J. Comparison of average crystallite size by X-ray peak broadening and Williamson–Hall and size–strain plots for VO2+ doped ZnS/CdS composite nanopowder. SN Appl. Sci. 1, 1509 (2019). https://doi.org/10.1007/s42452-019-1291-9
41. Fawad, M., Maqsood, N., Nawaz, A., Islam, B., Zaheer, M. D., & Skotnicová, K. (2025). Synthesis, Characterization, and Enhanced Optical and Dielectric Properties of Pure and Ni-Doped ZnO Nanoparticles for Advanced Electronic Applications. Results in Engineering, 26, 104824. https://doi.org/https://doi.org/10.1016/j.rineng.2025.104824
42. Li, Y., Yu, L., Pang, X., & Qin, G. (2025). Tuning stacking fault energy and enhancing mechanical properties of Al through Mg and Sc doping: Insights from density functional theory. Materials Today Communications, 43, 111639. https://doi.org/https://doi.org/10.1016/j.mtcomm.2025.111639
43. Fukamachi, S., Solís-Fernández, P., Kawahara, K., Tanaka, D., Otake, T., Lin, Y.-C., Suenaga, K., & Ago, H. (2023). Large-area synthesis and transfer of multilayer hexagonal boron nitride for enhanced graphene device arrays. Nature Electronics, 6(2), 126–136. https://doi.org/10.1038/s41928-022-00911-x
44. Yue, J., Huang, Y., Wang, X., Zhu, Y., Ragab, T., Jiang, K., Zhang, H., & Zhang, J. (2026). Surface Effects in Irradiation Damage: A Review of Underlying Multi-Scale Mechanisms and Cross-System Behaviors. Surfaces, 9(2), 40. https://doi.org/10.3390/surfaces9020040
45. Han, G., Zhang, D., Kong, C., Zhou, B., Shi, Y., Feng, Y., Liu, C., & Wang, D.-Y. (2022). Flexible, thermostable and flame-resistant epoxy-based thermally conductive layered films with aligned ionic liquid-wrapped boron nitride nanosheets via cyclic layer-by-layer blade-casting. Chemical Engineering Journal, 437, 135482. https://doi.org/https://doi.org/10.1016/j.cej.2022.135482
46. Wang, S., Song, X., Xu, J., Wang, J., & Yu, L. (2025). Flexible silicon for high-performance photovoltaics{,} photodetectors and bio-interfaced electronics. Mater. Horiz., 12(4), 1106–1132. https://doi.org/10.1039/D4MH01466A
47. Aktas, S., Hasanli, I. S., Demiroglu, A., & Caglar, M. (2024). Band gap tunability and optical properties of sol-gel derived Fe-doped CeO2 films. Physica B: Condensed Matter, 675, 415621. https://doi.org/https://doi.org/10.1016/j.physb.2023.415621
48. Jin, S., Zhang, M., Zeng, L., & Chen, D. (n.d.). Lanthanide-Doped Lead-Free Halide Double Perovskites: Optical Synergy, Performance Engineering, and Multifunctional Optoelectronics. Advanced Functional Materials, n/a(n/a), e32102. https://doi.org/https://doi.org/10.1002/adfm.202532102
49. Townsend, P. D., & Wang, Y. (2024). Improving interpretations of imperfections in insulating materials for current technologies. Optical Materials: X, 22, 100327. https://doi.org/https://doi.org/10.1016/j.omx.2024.100327
50. Bai, H., Qian, G., Liang, Q., Feng, Y., An, M., & Xie, Q. (2024). Tuning electronic and optical properties of two-dimensional vertical van der Waals blue Phosphorene/SnS2 heterostructure by strain and electric field. Computational Materials Science, 238, 112948. https://doi.org/https://doi.org/10.1016/j.commatsci.2024.112948
51. Sivakumar, V., Sivaganesh, D., Gopal, J. N., Muthuvinayagam, M., Kim, J. M., Kannan, P. K., & Saravanakumar, S. (2022). Enhancement of intrinsic green emission in phase pure ZnO. Physica B: Condensed Matter, 644, 414155. https://doi.org/https://doi.org/10.1016/j.physb.2022.414155
52. Han, J., Chen, T., Dong, Y., Deng, Z., Liu, Z., Zhao, Y., & Chen, A. (2026). Self-Powered Fast Response Flexible Ultraviolet Sensors Based on Reversible Deformed Nanowires for UV Communications Under Sunlight. Advanced Optical Materials, 14(14), e03354. https://doi.org/https://doi.org/10.1002/adom.202503354
53. Lee, J., Kumar, N., Patel, M., Ghosh, S., & Kim, J. (2023). Transparent metal-oxide personal UV monitoring device with machine learning advancement. Sensors and Actuators A: Physical, 362, 114627. https://doi.org/https://doi.org/10.1016/j.sna.2023.114627
54. Vavrinsky, E., Esfahani, N. E., Hausner, M., Kuzma, A., Rezo, V., Donoval, M., & Kosnacova, H. (2022). The Current State of Optical Sensors in Medical Wearables. Biosensors, 12(4), 217. https://doi.org/10.3390/bios12040217

55. Deng, B., Zhang, J., Gong, Y., Li, Z., Ruan, Y., Luo, H., & Zhou, F. (2025). Differences in Photocatalytic Performance and the Underlying Mechanisms of CaTiO3 Derived from Bauxite Residues Calcined at Different Temperatures. JOM. https://doi.org/10.1007/s11837-025-07793-2
56. Mohammed, K. S., Atlabachew, M., Aragaw, B. A., & Asmare, Z. G. (2024). Synthesis of Kaolin-Supported Nickel Oxide Composites for the Catalytic Oxidative Degradation of Methylene Blue Dye. ACS Omega, 9(4), 4287–4299. https://doi.org/10.1021/acsomega.3c05126
57. Han, G., Zhang, D., Kong, C., Zhou, B., Shi, Y., Feng, Y., Liu, C., & Wang, D.-Y. (2022). Flexible, thermostable and flame-resistant epoxy-based thermally conductive layered films with aligned ionic liquid-wrapped boron nitride nanosheets via cyclic layer-by-layer blade-casting. Chemical Engineering Journal, 437, 135482. https://doi.org/https://doi.org/10.1016/j.cej.2022.135482
58. Aydın, H., Çelik, S. Ü., & Bozkurt, A. (2017). Electrolyte loaded hexagonal boron nitride/polyacrylonitrile nanofibers for lithium ion battery application. Solid State Ionics, 309, 71–76. https://doi.org/https://doi.org/10.1016/j.ssi.2017.07.004
59. Wu, C., Soomro, A. M., Sun, F., Wang, H., Huang, Y., Wu, J., Liu, C., Yang, X., Gao, N., Chen, X., Kang, J., & Cai, D. (2016). Large-roll growth of 25-inch hexagonal BN monolayer film for self-release buffer layer of free-standing GaN wafer. Scientific Reports, 6(1), 34766. https://doi.org/10.1038/srep34766

Received: April 10th 2026 **Accepted: May 12th 2026**